12th International Conference on Fracture Mechanics of Concrete and Concrete Structures
FraMCoS-12
B.L.A. Pichler, Ch. Hellmich, P. Preinstorfer (Eds)

https://doi.org/10.21012/FC12.1148
MS17-2:3

EFFECT OF CRACK PATTERNS INDUCED BY DIFFERENT ACCELERATED TEMPERATURE ON MECHANICAL BEHAVIOR OF ASR-DAMAGED CONCRETE

HYO EUN JOO[*], JI XI[*] AND YUYA TAKAHASHI[*]

[*] The University of Tokyo, Bunkyo-ku, Tokyo, Japan
e-mail: joo@concrete.t.u-tokyo.ac.jp

Key words: Alkali-silica reaction, Crack pattern, Temperature, Compression, Image analysis

Abstract: Crack pattern induced by alkali-silica reaction (ASR) varies depending on environmental conditions, which affects the mechanical properties of concrete. This study aims to investigate the change in mechanical behaviors of ASR-damaged concrete with respect to acceleration temperature and crack pattern. Cylinder specimens were fabricated and immersed in 1 mol/L NaOH solution at two different temperatures, 40℃ and 60℃, for ASR acceleration until the expansions reached 0.25% and 0.50%. Subsequently, a cyclic compression test was performed to identify the elasticity and plasticity as well as the compressive strength and elastic modulus. In addition, using fluorescence epoxy-impregnated samples in each specimen, crack patterns due to ASR were observed under ultra-violet (UV) light and quantitatively analyzed through image analysis. The expansion rate of concrete stored at 60℃ was higher than that at 40℃, depending on which different ASR crack pattern and elastic modulus appeared. Large cracks were more prevalent in the specimen immersed at 40℃ than that at 60℃, and the reduction in elastic modulus of the specimen immersed at 60℃ was less than that at 40℃. The fracture parameters representing the remaining shear elasticity were calculated based on the measured elastic and plastic strains, and the results indicated that the fracture parameter of the specimen immersed at 40℃ was slightly lower than that at 60℃.

1 INTRODUCTION

In the mechanical performance of alkali-silica reaction (ASR) affected concrete, the strength and stiffness exhibit large differences even at the same expansion[1-4]. Although the relationships between these properties can be simplified through regression analysis, such approaches often result in overestimation or underestimation of concrete performance. Meanwhile, the previous test showed that the rate of ASR affected the mechanical properties of concrete. In Giaccio et al. (2008) and Abd-Elssmed et al. (2020)[1, 2], a slower reaction rate was associated with a smaller reduction in compressive strength and elastic modulus at the same level of expansion. This phenomenon may occur because the effect of hydration is greater than that of ASR in specimens with low reaction rates. However, according to existing test observations[1], the reaction rate changes ASR crack pattern; therefore, the crack pattern could be a primary factor influencing mechanical properties. When an ASR-affected concrete is subjected to an external load, the larger and more localized ASR cracks hinder stress transfer, even at the same ASR expansion.

This study aims to investigate the mechanical properties of ASR-damaged concrete with varying crack patterns caused by different reaction rates. To this end, a compression test was conducted on the

cylindrical concrete specimens damaged by ASR with different reaction rate. Two reaction rates were applied using different acceleration conditions (i.e., 1.0 N NaOH at 40 ºC and 1.0 N NaOH 60 ºC). Cyclic compression loading tests were performed to examine the elasticity, plasticity, and fracture behavior of the damaged concrete. Using the results of compression test, the differences in fracture progress, compressive strength, and elastic modulus of the specimens according to the reaction rate were compared. Additionally, crack pattern analysis was conducted to understand the tendency of the change in mechanical properties of ASR-affected concrete under varying crack patterns induced by different reaction rate.

2 METHODOLOGY

2.1 Test preparation

Cylinder specimens (ϕ 100 mm × h 200 mm) were manufactured with the designed mix proportion, where water to cement ratio (W/C) was 0.5, the sand was non-reactive (weight: 794 kg/m^3), and the reactive aggregate was andesite produced in Japan with the size of less than 20 mm (weight: 970 kg/m^3). NaOH pellets were added to mixing water to make 10 kg/m^3 Na_2O_{eq}. After casting concrete, all the specimens were kept in the controlled room (i.e., RH 60% and 20 ºC) for 1 year before ASR acceleration to reduce the effect of hydration; subsequently, they were stored in different conditions, as shown in Table 1. In the specimen label, the first letter means the damage level, where 'N', 'M', and 'H' indicate no damage, medium damage (i.e., target expansion of 0.2-0.25%), and high damage (i.e., target expansion of 0.45-0.55%), respectively. The temperatures followed by those letters, i.e., 20, 40, and 60 ºC, indicate the storage temperature during ASR acceleration period. For ASR acceleration, the M- and H- specimens were immersed in 1.0 N NaOH. 'CC', 'MC', and 'CR' indicate the type of experiment performed after the specimens reached the target expansion. 'CC' is the cyclic compression test, 'MC' is the monotonic compression test, and 'CR' is the crack observation test. As shown in Figure 1, the ASR expansion was measured until it reached the target expansion using a dial gauge on the measurement chips attached to the surface at intervals of 100 mm.

Table 1: List of test specimens

Specimen	Expansion (με)	Acceleration condition
N20°C−CC	0	RH 60%, 20 ºC
N20°C−MC	0	
M40°C−CC	2199	1.0N NaOH at 40 ºC
M40°C−CR	2144	
H40°C−CC	4650	
M60°C−CC	2536	1.0N NaOH at 60 ºC
M60°C−CR	5517	
H60°C−CC	2345	

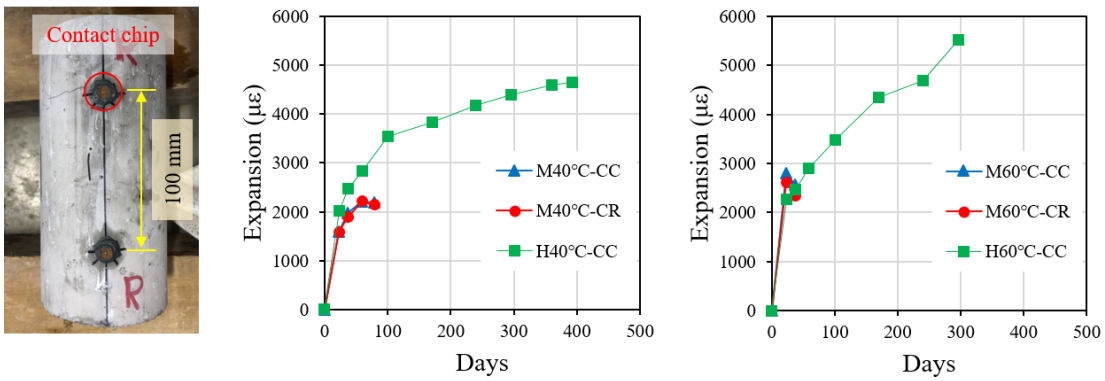

(a) Measurement method (b) Expansion at 40 ºC (c) Expansion at 60 ºC

Figure 1: ASR expansion measurement and progress

2.2 Compression test

As shown in Figure 2(a), a compressometer was used to measure the vertical strains, and two strain gauges were attached to measure circumferential strains. Cyclic compression test was carried out with a loading rate of 0.5 mm/min. In the initial stages of compression behavior, the applied load in each step was 5, 10, 20, 30, 40, and 50 kN, after which the load increased by 50 kN for each subsequent loading step until the maximum load. In post-peak region, the load was applied based on the longitudinal strain, i.e., for each loading step, the strain increased by 1000 microns from that in the previous step. The elastic modulus was calculated at the point of 40 % of compressive strength. In addition, the plastic strain (ε_p) was taken as the residual strain after unloading, and elastic strain (ε_e) was calculated by subtracting the plastic strain from the total strain (see Figure 2(b)).

2.3 Crack observation

The M40ºC−CR and M60ºC−CR specimens were cut into several slices, and the sliced samples were cleaned in ultrasonic bath with ethanol for 1 min; subsequently, they were kept at 40 ºC drying oven for 1 day and impregnated in fluorescence epoxy resin under the vacuum condition. Epodye was added to low-viscosity resin for making the fluorescence resin. As shown in Figure 3(a), the impregnated samples were polished by silicon carbide paper with gradually increasing grits from 180 to 1200 and diamond paste of 9, 6, 3, and 1 μm with oil-based lubricant. The samples were placed in the darkroom to observe cracks under ultra-violet (UV) light, as shown in Figure 3(b). A micro lens (Cannon EF-S35mm F2.8) was used for securing high resolution, and the irradiation intensity and wavelength of UV light were 2020 (μW/cm^2) and 254 nm, respectively.

3 TEST RESULTS

3.1 Compression test results

Figure 4 shows the change in compressive strength and elastic modulus according to ASR expansion. Compared to N-series, the compressive strength slightly increased in M-series (i.e., 0.2-0.25% exp.) and decreased in H-series (0.4-0.5% exp.). The elastic modulus showed clear decreasing trend with the expansion, and the reaction rate affected the reduction tendency of elastic modulus. The 60 ºC series specimens (i.e., high reaction rate) had less reduction in elastic modulus than the 40 ºC series specimens (i.e., low reaction rate). This result can be explained through crack patterns, which are discussed in section 3.2.

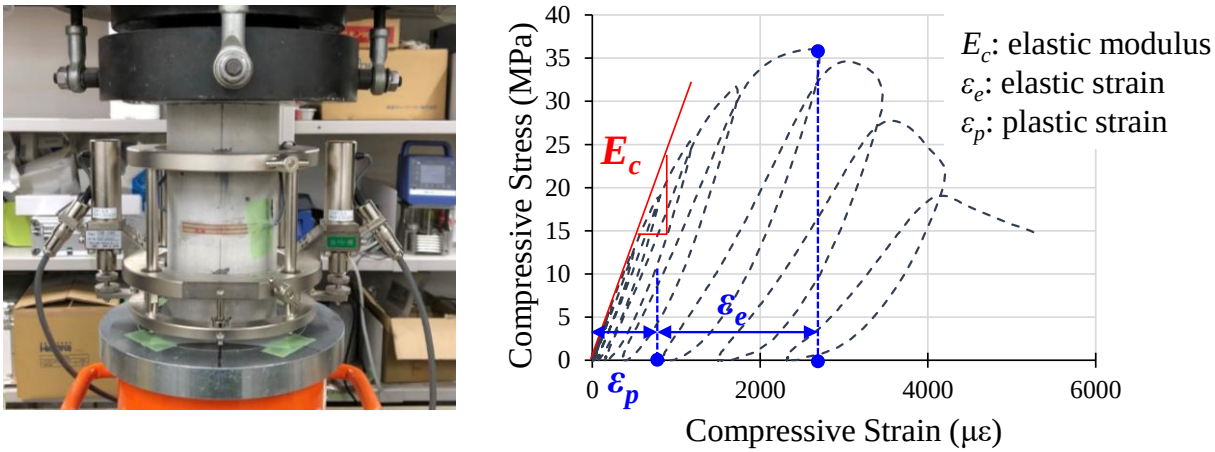

(a) Photo of compression test (b) Cyclic compression test

Figure 2: Methods for compression test

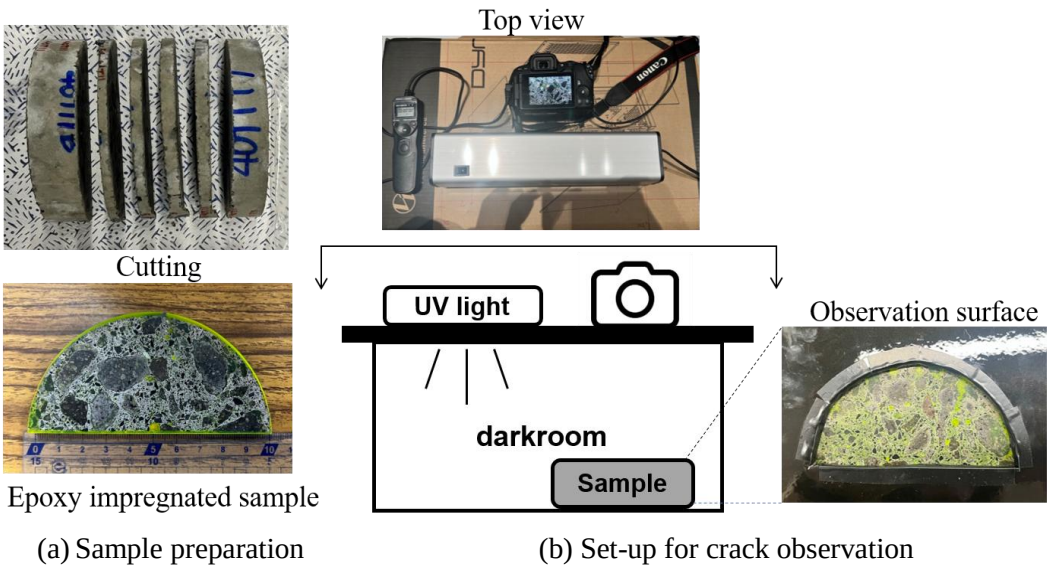

Figure 3: Methods for compression test

The results of cyclic compression tests are represented in Figure 5. Comparing the compression curves of N20ºC−CC and N20ºC −MC in Figure 5(a), the repeated loading did not reduce compressive strength and elastic modulus. In M- and H-series, the elastic modulus and compressive strength showed a tendency to decrease as the expansion increased, as shown in Figure 5 (b) and (c). In addition, the compressive strain increased rapidly as the expansion increased; accordingly, both elastic and plastic strains slightly increased with the expansions, as presented in Figure 6.

To evaluate the continuum fracture based on elastic and plastic strain behaviors, the fracture parameter (K) was adopted from Maekawa et al. (1993)[5], which can be calculated, as follows:

$$K = J_2 / (2G_o J_{2e}) \quad (1a)$$

$$K = (J_2 / f_{2ck}) / (J_{2e} / \varepsilon_o (1+\nu)) \quad (1b)$$

where, J_2 is the second invariant of deviatoric stress, J_{2e} is the elastic deviator invariant, G_o is the elastic shear modulus, f_{ck} is the compressive strength, ε_o is the strain corresponding to f_{ck}, and ν is the Poisson ratio. In general, concrete loses its shear elasticity as the damage progresses; thus, K is a quantifiable value for the damage progress and represents the remaining spring against shear, as presented in Figure 7(a)[5]. The second invariants were calculated through the measured plastic and elastic strains, and the details of calculation can be found in [5]. The calculation results showed that the fracture parameters (K) were almost the same regardless of expansion level and reaction rate, as shown in Figure 7(b). This indicates that the fracture progress in concrete subjected to compression does not change after ASR expansion under no confinement, even though the compressive strength and elastic modulus can be reduced by ASR. In the following section, the changes in mechanical performance of concrete are examined based on the crack pattern analysis.

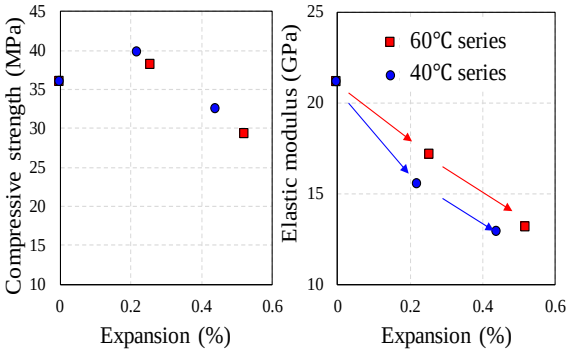

Figure 4 Compressive strength and elastic modulus with respect to expansion

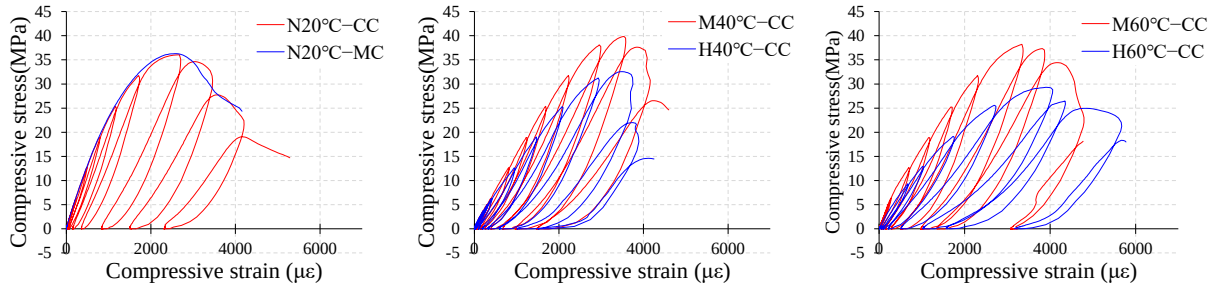

(a) 20°C series specimens (b) 40°C series specimens (c) 60°C series specimens

Figure 5: Cyclic compression test results

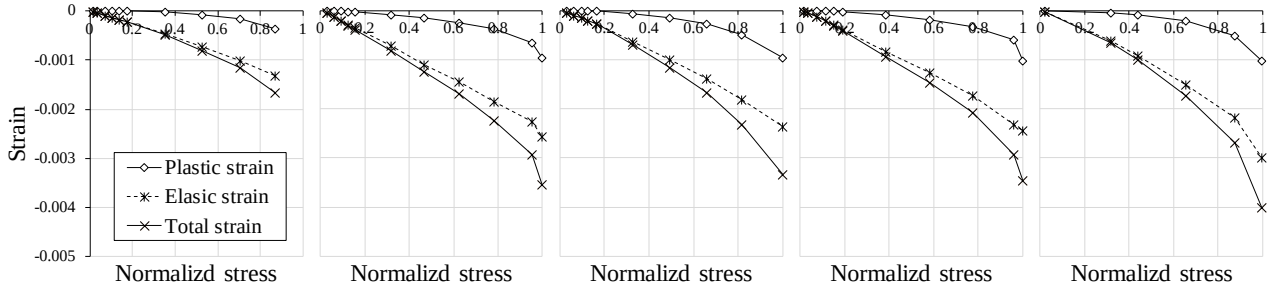

(a) N20°C−CC (b) M40°C−CC (c) M60°C−CC (d) H40°C−CC (e) H60°C−CC

Figure 6: Elastic and plastic strain behaviors

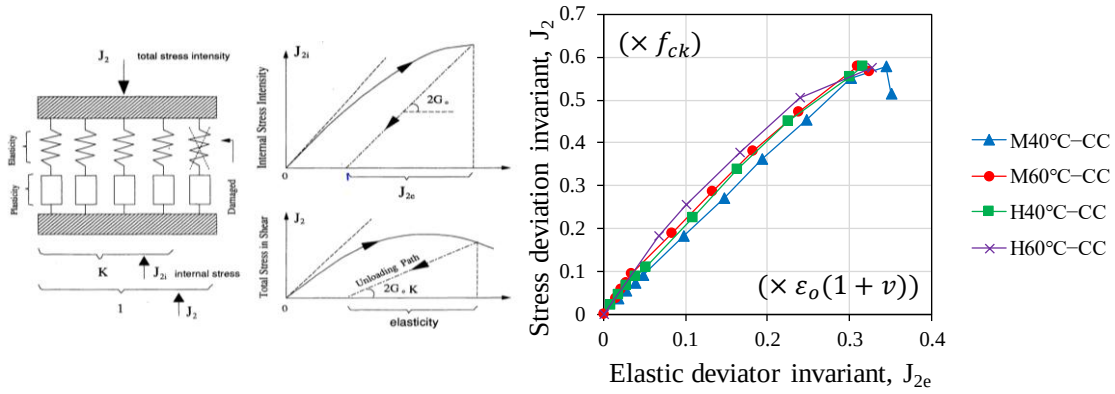

(a) Scheme for fracture system [5] (b) Results of fracture progress

Figure 7: Elastic and plastic strain behaviors

3.2 Crack observation

One of the images taken under UV light is shown in Figure 8(a), where cracks and pores appear brighter than other areas. The crack, pore, aggregate, and cement paste were segmented from the image by using the interactive learning and segmentation toolkit (ilastik[6]) which is based on the machine learning algorithm. Figure 8(b) shows the segmented crack distribution. To remove the noise and connect the close pixels, image processing was conducted by utilizing image J and scikit-image in python package[7]. Then, the crack size distribution was calculated using Porespy[8], as shown in Figure 8(c). Figure 9 shows the crack size distribution in M40-2 and M60-2 specimens. The portions of large size cracks are greater in M40 (i.e., low reaction rate) than those in M60 (i.e., high reaction rate). Thus, it is estimated that the crack size and its distribution resulted in different reductions in elastic modulus. The M40 with large cracks exhibited greater reduction in elastic modulus than M60. The reason for the overall crack area to be smaller in M60 than M40 might be because of the limit in the range of detectable

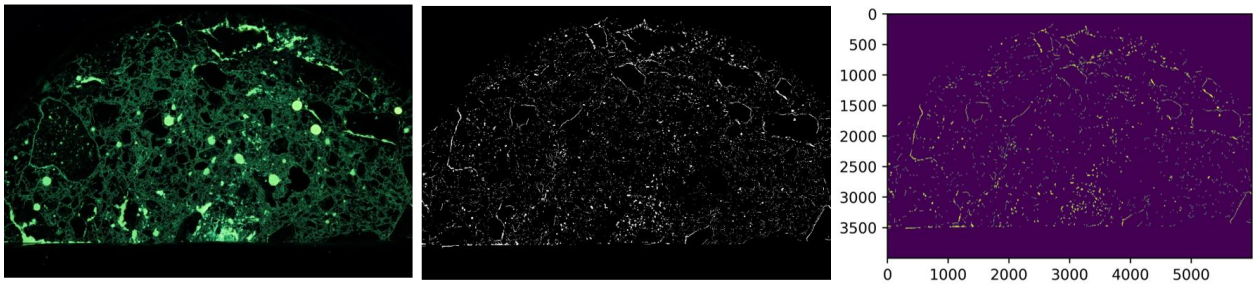

(a) Photo taken by camera (b) Segmented image (c) Analyzed image [unit: pixel]

Figure 8: Image analysis procedures

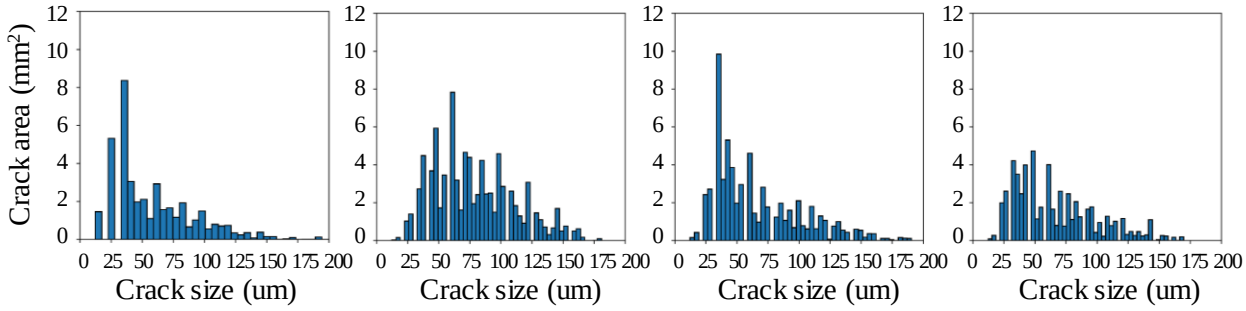

(a) M40 ºC−CR

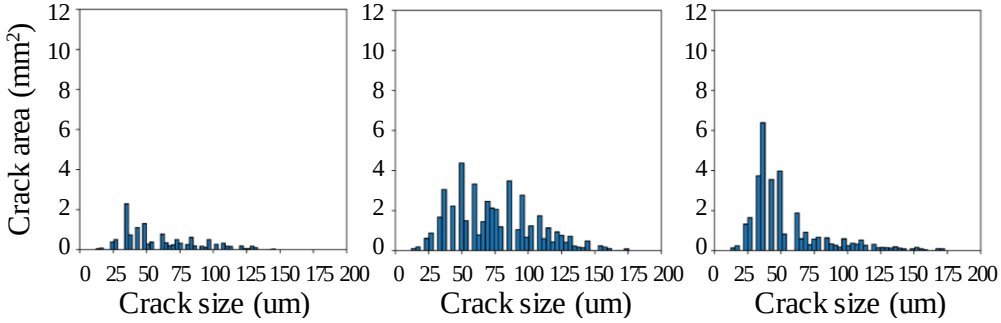

(b) M60 ºC−CR

Figure 9: Analyzed crack size distribution

crack size. Due to the resolution of image, cracks with a size of less than 25 μm could not be detected; thus, M60 specimen might have larger number of small cracks in those range (i.e., crack size ≤ 25 μm).

Based on the experimental results, the mechanical properties of ASR-affected concrete can be changed depending on the crack patterns even if the expansion was the same. It can be explained through the stress transfer mechanism with respect to different crack patterns. The larger the crack size is, the more difficult it is to transfer stress. Although the damage rating index (DRI)[9], which is known for microscopic assessment of damage, considers the location of cracks, this study suggests the importance of investigation on crack size distribution to evaluate the performance of ASR-affected concrete. To strengthen the conclusions, additional experiments with various ASR conditions need to be conducted. In addition, the mechanism causing different crack patterns needs to be further studied.

4 CONCLUSIONS

This study investigated the change in mechanical properties of ASR-affected concrete, such as fracture progress,

compressive strength and elastic modulus, according to the reaction rate based on the crack size distribution. The conclusions obtained from this study are:

1. As the ASR expansion increased, total compressive strain and elastic and plastic strains increased; however, the fracture parameter representing the remaining shear elasticity of concrete did not change according to ASR damage.
2. This means that the fracture progress in concrete subjected to compression does not change after ASR damage under no confinement, even though the compressive strength and elastic modulus can be reduced by ASR.
3. The elastic modulus showed clear decreasing trend with the expansion, and the reaction rate affected the reduction tendency of elastic modulus.
4. It is estimated from the observed crack distribution that the crack size and its distribution resulted in different reduction in elastic modulus. The M40 specimen (low reaction rate) with large cracks exhibited greater reduction in elastic modulus than M60 specimen (high reaction rate).
5. To evaluate the mechanical performance of ASR-affected concrete, not only the amount of ASR expansion but also the crack patterns should be considered as one of the key factors.

ACKNOWLEDGEMENT

This study was financially supported by Japan Science and Technology Agency through the Fusion-Oriented Research for Disruptive Science and Technology Program (Grant No. JPMJFR225V), as well as JSPS KAKENHI Grant No. 21H01416.

REFERENCES

[1] Giaccio, G., Zerbino, R., Ponce, J.M., Batic, O.R., 2008. Mechanical behavior of concretes damaged by alkali-silica reaction. *Cem. Concr. Res.* **38**: 993–1004.

[2] Abd-Elssamd, A., Ma, Z.J., Le Pape, Y., Hayes, N.W., Guimaraes, M., 2006. Effect of Alkali-Silica Reaction Expansion Rate and Confinement on Concrete Degradation. *ACI Material Journal.* **117**: 265-277.

[3] Ji, X., Joo, H.E., Yang, Z., Takahashi, Y., 2021. Time-dependent Effect of Expansion due to Alkali-silica Reaction on Mechanical properties of Concrete. *J. Adv. Concr. Technol.* **19**: 714–729.

[4] Kishira, R., Maeshima, T., Koda, Y., Iwaki, I., 2021. Invesitigation on punching shear capacity of RC deck slab attacked by ASR for four years on steel girders. *J. JSCE.* **67A**.

[5] Maekawa, K., Okamura, H., Pimanmas, A., 2003. *Non-Linear Mechanics of Reinforced Concrete.* CRC Press.

[6] Berg, S., Kutra, D., Kroeger, T., Straehle, C.N., Kausler, B.X., Haubold, C., Schiegg, M., Ales, J., Beier, T., Rudy, M., Eren, K., Cervantes, J.I., Xu, B., Beuttenmueller, F., Wolny, A., Zhang, C., Koethe, U., Hamprecht, F.A., Kreshuk, A., 2019. ilastik: interactive machine learning for (bio) image analysis. *Nat. Methods.* **16**: 1226–1232.

[7] Walt, S., Schönberger, J.L., Nunez-Iglesias, J., Boulogne, F., Warner, J.D., Yager, N., Gouillart, E., Yu, T., scikit-image: image processing in Python. *PeerJ*. **2**: e453.

[8] Gostick, J., Khan, Z., Tranter, T., Kok, M., Agnaou, M., Sadeghi, M., Jervis, R., 2019, PoreSpy: A Python Toolkit for Quantitative Analysis of Porous Media Images. *J. Open Source Softw.* **4**: 1296.

[9]Sanchez, L.F.M., Fournier, B., Jolin, M., Mitchell, D., Bastien, J., 2017. Overall assessment of Alkali-Aggregate Reaction (AAR) in concretes presenting different strengths and incorporating a wide range of reactive aggregate types and natures. *Cem. Concr. Res.* **93**: 17–31.